ORIGINAL ARTICLE

Synthesis of lanthanum-modified clay soil-based adsorbent for the fluoride removal from an aqueous solution and groundwater through batch and column process: mechanism and kinetics

Chandra Bhan[1] · Jiwan Singh[1] · Yogesh Chandra Sharma[2] · Janardhan Reddy Koduru[3]

Abstract

In the present work, pond clay was modified with lanthanum and applied for fluoride uptake from an aqueous environment. The clay soil was treated with a 0.1 M solution of lanthanum oxide and heated at 500 °C for 90 min in a muffle furnace. The modified clay was characterized by the following techniques: particle size analysis, zeta potential, Fourier-transform infrared, scanning electron microscopy, transmission electron microscopy, pH at the zero point of charge, X-ray diffraction, Brunauer–Emmett–Teller, and X-ray photoelectron spectroscopy. The adsorption experiments revealed that modified clay soil was very effective in removing fluoride with an adsorption capacity of 1.96 mg/g. The fluoride removal was followed well with Langmuir isotherm ($R^2 = 0.999$), pseudo-second-order kinetics ($R^2 = 1$), and the adsorption was an exothermic process. The performance of lanthanum-modified clay (LMC) in a fixed bed column was evaluated using different models, including the Thomas, Adams–Bohart, Yoon–Nelson, and Clark models. A regeneration study was compared with NaOH and $NaHCO_3$ and successfully performed for four adsorption cycles. A probable mechanism is proposed including ligand exchange, electrostatic attraction, and inner complexation for fluoride adsorption on the LMC. The developed adsorbent was also tested for the treatment of natural groundwater.

Keywords Adsorption · Clay soil · Column study · Fluoride · Lanthanum-modified clay · XPS

Introduction

Soil and its minerals, which are provided by nature, are used for various human practices. The clay soil is formed by the gradual weathering of rock materials and is deposited in the lower region. Clay was deposited at the bottom of the pond and has also been used for the preparation of earthen pots in villages. Because of its good ion exchange capacity, clay soil has been used for adsorption purposes (Adeyemo et al. 2017; Lambert 2018; Shen and Gao 2019). Many researchers have employed clay-based adsorbents for the removal of harmful chemical contaminants from wastewater. Groundwater is contaminated with inorganic and organic pollutants. Fluoride contamination has been reported in various regions of the world (Atasoy et al. 2013; Yadav et al. 2019; Karunanidhi et al. 2019). Owing to the intake of fluoride-containing water, approximately 411 million people are at risk and more than 66 million people are facing health problems of fluorosis, of which 6 million are children. Fluoride contamination in groundwater sources is a major risk to human health, mainly in rural areas of developing countries (Mukherjee and Singh 2020). Approximately 200 million people from 25 countries, including China, India, Pakistan, Iran, Mexico, Thailand, and West and Southern Africa, face the fate of dental and skeletal fluorosis (Mumtaz et al. 2015; Kadam et al. 2020). In particular, because of the consumption of untreated groundwater, a large population of rural India is suffering from fluorosis (Adimalla et al. 2019). Fluoride-containing minerals, such as apatite, biotite, cyolite, fluorite, sellite, topaz, kaolinite, and fluocelite, are the natural causes

✉ Jiwan Singh
jiwansingh95@gmail.com

✉ Janardhan Reddy Koduru
reddyjchem@gmail.com

[1] Department of Environmental Science, Babasaheb Bhimrao Ambedkar University, Lucknow 226025, India

[2] Department of Chemistry, Indian Institute of Technology (BHU), Varanasi 221005, India

[3] Department of Environmental Engineering, Kwangwoon University, Seoul 139-701, Republic of Korea

of fluoride pollution in groundwater (Mukherjee and Singh 2018; Hanse et al. 2019). The dissolution of these minerals release fluoride ions in groundwater (Mobarak et al. 2018; Enalou et al. 2018). Moreover, effluents containing a high concentration of fluoride released from different types of industries include semiconductor manufacturing, coal-based power units, iron smelters, glass, electroplating, ceramic, and brick processing units; these effluents pollute surface water and groundwater (Bharti et al. 2017; Preethi and Meenakshi 2018). Various treatment technologies for the defluorination of water include precipitation, reverse osmosis, nanofiltration, ion exchange, electrodialysis, and adsorption (Singh et al. 2016; Nagaraj et al. 2020). But there are some limitations with these fluoride removal methods that are discussed. The chemical precipitation method is easy to understand, it needs a high amount of $Al(OH)_3$ (700–1200 mg/L) and generates a large quantity of sludge that is the issue of its transfer (Jagpat et al. 2012). Membrane filtration involves mainly nanofiltration and reverse osmosis, it requires to continue electric energy and has the chance of membrane fouling (Akafu et al. 2019). In the electrodialysis method, fluoride ions passed through a semipermeable membrane under influence of electric potential. It is easily affected by co-existing ions and also this is a costly process (Majewska-Nowak et al. 2015). Ion exchange has high efficiency (90–95%) but the presence of carbonate, sulfate, and phosphate ions affects its efficiency. This is a costly technique and fluoride loaded resins and their regeneration is a problem (Waghmare and Arfin 2015). Adsorption is considered a good method because of its cost-effectiveness and comfortable operation (Ghosal et al. 2015; Mei et al. 2020).

Different adsorbents have been applied for the elimination of fluoride ions, such as biosorbents, zeolite carbonaceous materials (Fito et al. 2019), clay minerals (Uddin et al. 2019), iron and alumina, modified charcoal (Wendimu et al. 2017), and calcium-activated biochar (Zhang et al. 2020). Adsorptive properties depend on their physicochemical characteristics, such as crystal size, surface area, porosity, composition, and ion exchange capacity (Mudzielwana et al. 2018); these properties can be modified by chemical and heat treatment to improve the adsorptive capacity (Garcia-Sanchez et al. 2016). The number of adsorbents has been chemically modified to improve fluoride uptake, such as activated carbon by Fe and Al (Solanki et al. 2019), magnetic biochar Fe_2O_3/Fe_3O_4 treatment (Dewage et al. 2018), aluminum, magnesium, and titanium modified natural zeolite (Ma et al. 2018), and bentonite treated with Mn^{2+} (Mudzielwana et al. 2018). Moreover, aluminum oxide-modified clays (Dessalegne et al. 2018) and Fe^{3+}-modified clinoptilolite/montmorillonite (Corral-Capulin et al. 2019) have been used. Lanthanum has been found very effective for fluoride adsorption due to its high electron affinity compared to other rare earth metals (Nagaraj et al. 2017) and it

is also low cost as $4/1000 g of commercial grade (Yang et al. 2019). Therefore, we have chosen lanthanum as good elemental species and used it for modification of clay soil, and applied it for the elimination of fluoride through batch adsorption and continuous adsorption in a fixed bed column. In some adsorption work such as Kofa et al. (2017), Nabbou et al. (2019), Ayalew et al. (2020) performed the adsorption studies only for optimization of adsorption conditions, not as continuous adsorption, but in this work, application of pond clay soil as adsorbent for fluoride removal by continuous as well as working mode adsorption in a fixed bed column were studied that is the novelty of this work. Clay soil may be an alternative to commercially available clay minerals for adsorbent preparation; furthermore, it is immensely cheap because of its large availability in ponds.

Materials and methods

Materials

The clay soil sample was collected from a pond located in the village of Rampur, Ambedkar Nagar Uttar Pradesh, India (26°19′51″ N, 83°03′33″ E). Lanthanum oxide, hydrochloric acid, sodium hydroxide, and sodium chloride were obtained from Fisher Scientific. Fluoride solution (1000 mg/L) and ionic strength adjustor (ISA) solutions were obtained from Antech.

Quality control and assurance

Confirmation of clay soil in the collected sample was done by grain size analysis using CILAS instrument Laser Particle Size Analysis Cilas 1190 (Cilas SA or leans, France). The obtained data were applied to determine grain size parameters of soil sample using GRADISTAT software (Blott and Pye 2001). The graphical representation of data was done by using the above-mentioned software. Acquired data (Fig. S2) revealed that very fine sand 47.9% and 52.1 % mud (very coarse silt 33.0%, medium silt 4.6%, fine silt 3.7%, very fine silt 3.2 and clay 2.3%) are present in the sample.

Preparation of lanthanum-modified clay

The collected clay soil was crushed using a mortar pestle and converted into a fine powder. The powder was filtered with a 250 μm sieve, washed with distilled water, and dried in an oven. A total of 15 g clay soil was mixed with 100 mL of a 0.1 M lanthanum oxide solution, and the mixture was stirred for 2 h. The mixed material was dried and placed in a muffle furnace at 500 ℃ for heat treatment. The heated clay was repeatedly cleaned using distilled water and kept in a hot-air oven for drying overnight. This modified clay

soil was stored in a reagent bottle and used for removing fluoride from an aqueous solution. The prepared adsorbent was named lanthanum-modified clay (LMC).

Characterization of the LMC

Morphological and elemental analyses of the raw clay and LMC were analyzed by scanning electron microscopy (SEM, JSM 4490, JEOL JAPAN) facilitated with energy-dispersive X-ray spectroscopy (EDS), and these characteristics were also investigated by transmission electron microscopy (TEM, JEOL). The available or existing charged species on the LMC surface at a specific pH was confirmed using the pH at the zero point of charge (pHzpc) test. This test was performed with 50 mL of 0.01 M NaCl solution with 0.02 g of modified clay, and different pH values (2, 4, 6, 8, and 10) were set using a solution of 0.1 M HCl and 0.1 M NaOH. The pH of all solutions with the LMC composite was checked after 48 h using Water Analyzer 371, Systronics, and the graph was obtained between the initial and final pH (pH of the solution with adsorbent). Zeta potential and particle size analysis were performed using Zeta Nanosizer (Nano-ZS90, Malvern). The available functional groups were characterized by Fourier-transform infrared (FTIR) analysis in the range 400–4000 cm^{-1} using NICOLET 6700 THERMO SCIENTIFIC, USA. The crystalline nature of raw clay and LMC was confirmed by X-ray diffraction (XRD) (Bruker D8 ADVANCE eco, Japan). The surface area and pore volume of LMC were analyzed by the adsorption and desorption of nitrogen using Brunauer–Emmett–Teller (BET) method (BEL Japan, Inc.). The temperature was 293 K for N$_2$ adsorption and 200 K for desorption during the BET analysis. The available elements in the raw clay soil, LMC, and LMC after fluoride adsorption was analyzed using X-ray photoelectron spectroscopy (XPS) (K-Alpha, Thermo Scientific).

Adsorption experiment by batch process

All the adsorption studies were conducted using the batch process in a 250 mL Erlenmeyer flask with 50 mL aqueous solution shaken at a constant orbital speed of 80 rpm. All experiments were performed at room temperature, except for the temperature studies. The samples were collected at a predetermined time and filtered using Whatman filter paper. A total of 0.5 mL ISA solution was added to the collected sample to fix the F$^-$ concentration. The remaining fluoride concentration was analyzed using a selective ion electrode (EUTECH ION 6+, Thermo Scientific, USA). Experiments were conducted using triplet samples to minimize possible errors. Suitable conditions for the optimization of the experiment using different doses (1–6 g/L), contact time (5–120

min), solution pH (4–10), starting concentration of fluoride (5–20 mg/L), and temperature (25–55 ℃).

The quantity of fluoride (*q* in mg/g) adsorbed at saturation time and adsorption percentage (*R*%) were calculated using Eqs. (1) and (2), respectively.

$$q = \frac{(C_0 - C_t)}{m}V, \tag{1}$$

$$R\% = \frac{(C_0 - C_t)}{C_0} \times 100, \tag{2}$$

where C_0, V, m, and C_t denote the initial concentration of fluoride (mg/L), volume (L), dry amount of LMC (g), and residual fluoride concentration (mg/L) after a specific time, respectively.

Adsorption experiment by a continuous process

A continuous adsorption experiment was performed for the adsorption of fluoride on La-clay composites using a borosilicate column designed and reported by Sahu et al. (2020a, b). Experimental parameters such as neutral pH and room temperature were maintained throughout the study. Two different depths (3 cm and 6 cm) of the adsorbent were fixed in the column. The 0.5 cm adsorbent bed was fixed and a cotton layer was kept between each adsorbent bed to simplify the flow rate; a schematic illustration of the column is shown in Fig. 1. The total adsorbent bed depth, excluding the cotton layer, was 3 cm and 6 cm. A fluoride solution containing 10 mg/L was passed through the column at an inlet flow rate of
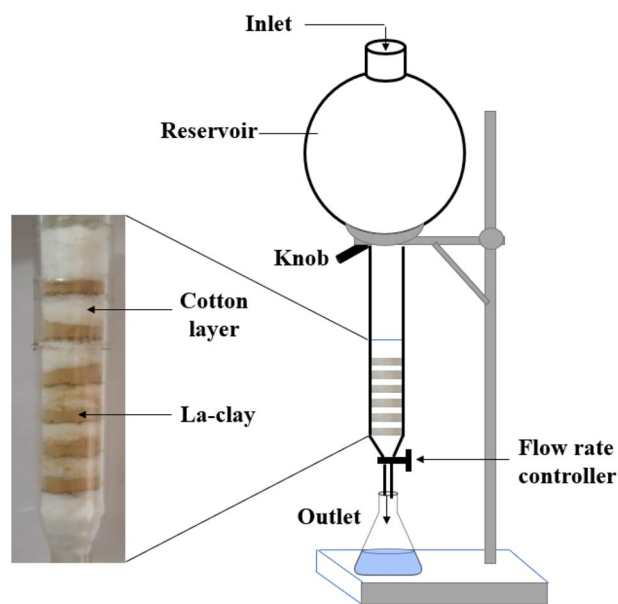

Fig. 1 Schematic diagram of fixed bed column.

5 mL/min and 10 mL/min. The main aim of the continuous adsorption experiment was to check the adsorption capacity of a fixed amount of LMC for aqueous solution treatment.

Column parameters analysis

Breakthrough curve The concept of the breakthrough curve for continuous adsorption is described for a fixed bed column. This is an important characteristic for evaluating the dynamic response and operation of the adsorption column. C_t/C_0 was plotted against time to check the behavior of fluoride adsorbed from the inlet solution in a fixed bed.

The total volume of the treated solution can be evaluated by the following equation:

$$V_{eff} = Q \times t_{total}, \tag{3}$$

Here, V_{eff} denotes the total outlet volume, Q represents the flow rate of the solution, and t_{total} denotes the total flow time.

The total amount of fluoride adsorbed on the fixed adsorbent can be calculated as follows:

$$q_{total} = \frac{Q}{1000} \int_{t=0}^{t=total} C_{ad} dt, \tag{4}$$

The adsorption capacity of the adsorbent in the column is given below.

$$q_e = \frac{q_{total}}{m}, \tag{5}$$

Here, q_e is the adsorption capacity and m are the dry amount of LMC fixed in the column.

The total delivered amount of fluoride in the column is given by,

$$M_{total} = t_{total} \times C_0 \times Q. \tag{6}$$

Results and discussion

Characterization of developed adsorbent

Morphological analysis

SEM was used to analyze the morphological structure (shape and size) of the raw clay and LMC. The surface morphologies of the natural clay and LMC are shown in Fig. 2a, c. Natural clay contains small particles with significantly varying sizes. In contrast, natural clay has a flaky particle shape, whereas modified clay has a comparatively large and clumped flaky shape and rough surface. The clumping of clay particles might be happened due to the fusion of small particles under the influence of high temperature (500 ℃). A similar result was reported by Elgamouz et al. (2019).

The natural clay and modified clay were characterized using EDS. The EDS maps of natural clay confirmed that its surface contained O, Mg, Al, Si, K, Ti, and Fe with weight percentages of 50.71%, 2.84%, 12.51%, 22.70%, 3.18%, 2.23%, and 5.83%, respectively. Meanwhile, the percentage of these components decreased in the LMC, as shown in Fig. 2d. The peaks in the EDS maps confirmed the successful binding of lanthanum to the clay surface. SEM image of the LMC after fluoride adsorption appeared smooth flaky structure and EDS analysis (Fig. 2e, f) revealed that fluoride ions well adsorbed on the LMC surface. The internal appearance, such as the shape and size of raw clay soil and LMC soil were investigated by TEM analysis (Fig. 2g, h). Raw clay looks like a nanorod with a flaky structure and a size of 84 nm to 159 nm. Lanthanum-containing clay had a few alterations due to heat treatment at 500 ℃. The particle size of the LMC was 255–288 nm.

FTIR analysis

FTIR analysis is the most important technique for confirming the functional groups available on the exterior region of the raw clay and LMC. The peaks at 435 cm^{-1} and 787.2 cm^{-1} represent Si–O–Si-bending vibration. The peaks at 1179.3 cm^{-1} and 1634 cm^{-1} contribute to the Si–O stretching region and OH deformation of water, respectively (Bukalo et al. 2017). Figure 3a shows the spectrum of the functional groups present in the clay soil and LMC. The wavenumber 3619 cm^{-1} determines the OH stretching of inner hydroxyl group of kaolinite (Bukalo et al. 2017). In LMC, the wavenumbers 422 cm^{-1} and 474 cm^{-1} confirm Si–O deformation and Si–O–Si deformation, respectively, and these bonds are shifted from their original positions. The stretching region (Si–O) was observed at the peaks 787 cm^{-1}, 1016.9 cm^{-1}, and 1100 cm^{-1} (Madejova et al. 2017). At 3619 cm^{-1} the OH band intensity decreased after adsorption of fluoride and also significant changes were observed of all peaks in the range of 1634–400 cm^{-1} compared to LMC peaks. These alterations in the peaks confirm that OH groups and metal ions present on the surface of LMC interacted with fluoride ions.

XRD analysis

The diffractogram acquired for the natural pond clay and LMC is shown in Fig. 3b. The XRD pattern revealed that montmorillonite was present at 2θ = 8.9° (Castro et al. 2019). The peaks at 2θ = 18°, 2θ =21°, 2θ =25°, and 2θ = 25.5° confirm the presence of illite, quartz, and kaolinite, respectively (Saeed et al. 2015; Nabbou et al. 2019; Liu et al. 2019). Illite, quartz, and kaolinite are also present in the raw clay with the peaks at 2θ = 45°, 2θ =50°, and 2θ = 55°, respectively (Saeed et al. 2013; Saeed et al. 2015).
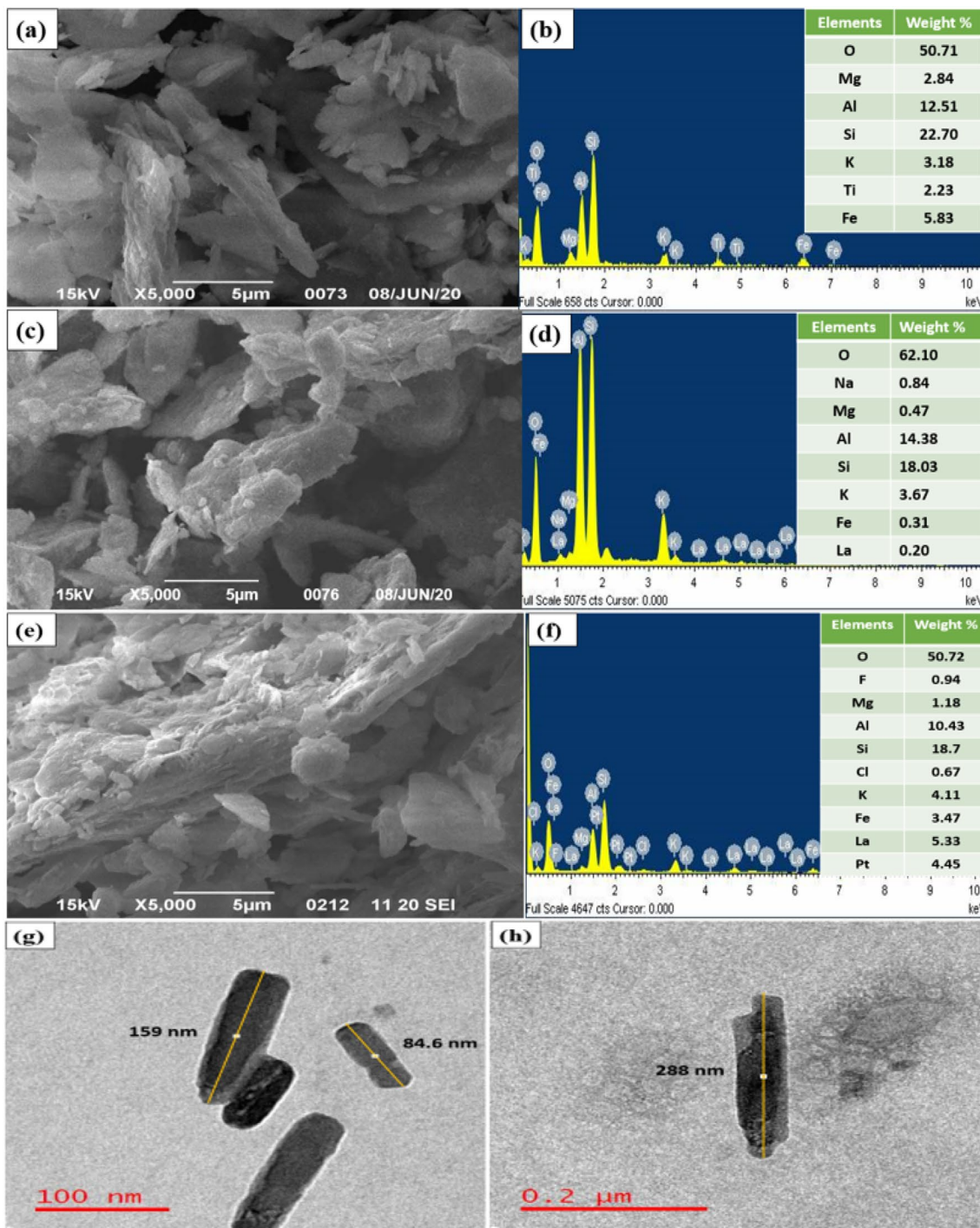
Fig. 2 Scanning electron microscopy (**a**, **c** and **e**) and energy-dispersive X-ray spectroscopy (**b**, **d** and **f**) analysis of raw clay soil; lanthanum-modified clay (LMC) and LMC after fluoride adsorption. Transmission electron microscopy analysis of raw clay (**g**) and LMC (**h**)

The little alteration occurred in the crystalline phase of LMC clay. Significant changes can be observed clearly at peaks range from $2\theta = 18.2°$ to $2\theta = 61.4°$ in LMC after fluoride adsorption. The large peak at $19.5°$ has been shifted to $32.1°$ having high intensity.

pHzpc of LMC

The pHzpc analysis provides information about the acid/base nature of the adsorbent, which affects the pH of the solution and the electrostatic interaction between the adsorbed
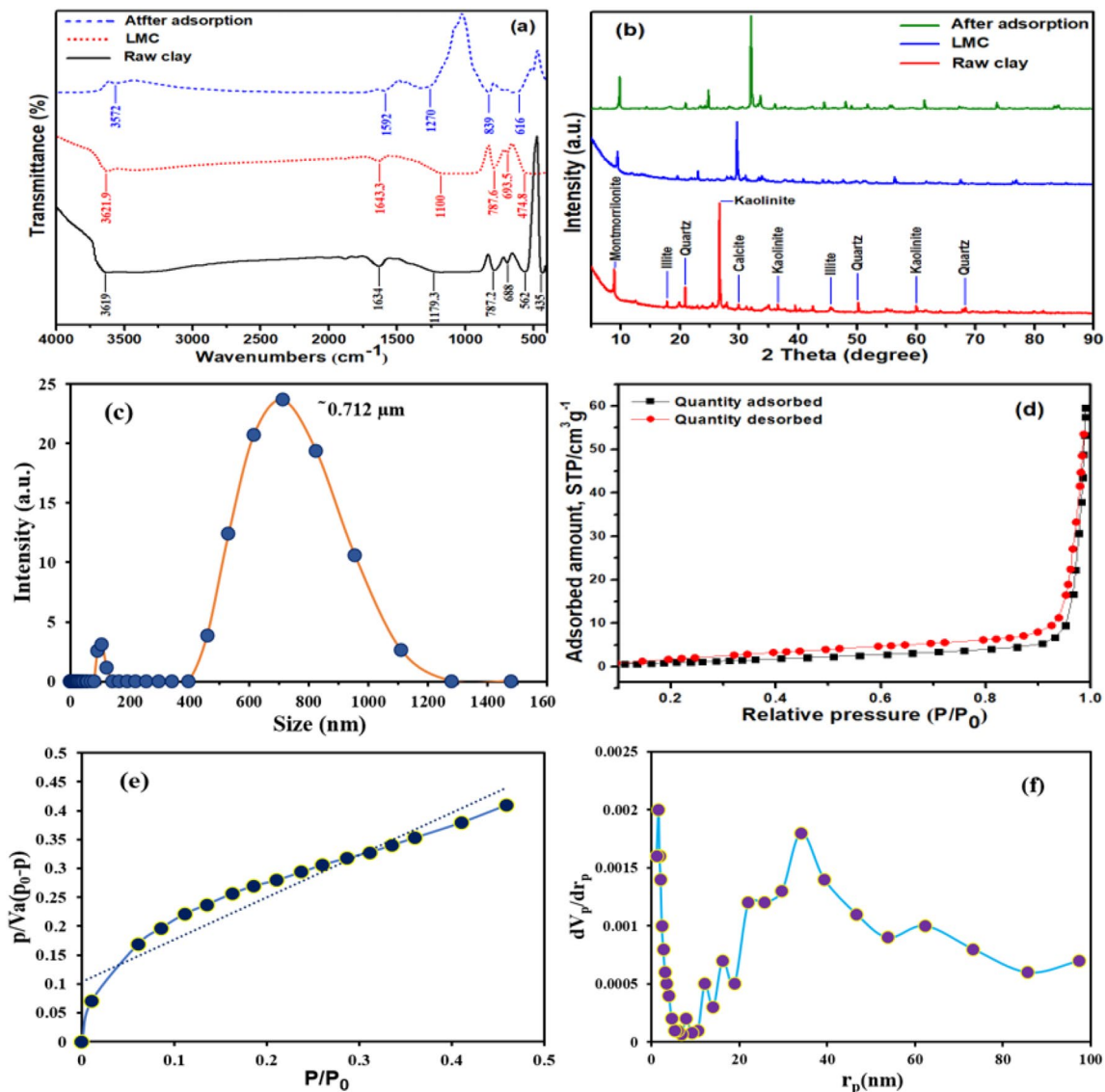
Fig. 3 Fourier-transform infrared spectra (**a**), X-ray diffraction analysis (**b**), PSA analysis (**c**), N_2 adsorption/desorption curve (**d**), Brunauer–Emmett–Teller plot (**e**), and Barrett–Joyner–Halenda curve (**f**)

ions and charges present on the adsorbent surface. The pHzpc determines the pH at which the total surface charge of the adsorbent is electrically neutral. The adsorbent surface contains a positive charge when the pH becomes less than pHzpc, while the adsorbent surface contains negatively charged species when the pH exceeds pHzpc (Raghav and Kumar 2018). The pHzpc of the LMC was found to be 6, confirming that its surface was positively charged (Fig. S2a).

Zeta potential and particle size analysis

A high positive or negative zeta potential value of the adsorbent indicates the good physical stability of particle suspensions because of the electrostatic repulsion between

particles. Zeta potentials lower than – 30 mV and higher than + 30 mV create repulsive forces that maintain colloidal stability. The zeta potential of the LMC was + 25.1 mV at pH 2 presented in Fig. S2b. The particle size of the LMC was 600–1000 nm, and the maximum intensity was found for a 0.712 μm particle size (Fig. 3c).

N$_2$ adsorption/desorption analysis

LMC was characterized by the adsorption/desorption of N_2 (Fig. 3d, f). The pore volume, surface area, and pore diameter were also determined. Type IV N_2 adsorption–desorption isotherm having type-H_3 hysteresis appeared for LMC, which is classified according to the international union of

pure and applied chemistry. The same type of adsorption isotherm was reported by Caponi et al. (2017) in the adsorption/desorption isotherm. The BET surface area of LMC was 6.54 m^2/g, while the mean pore diameter and total pore volume were 55.510 nm and 0.0914 cm^3/g, respectively. The large surface area facilitated the adsorption of fluoride ions.

XPS

The XPS data of the raw clay soil, LMC, and LMC after fluoride adsorption are shown in Fig. 4. The Al2p (74.2 eV), Si2p (101.5 eV), C1s (283.2 eV), O1s (531.8 eV), Fe2p (711.8 eV), and Mg1s (1303.1 eV) peaks were present in the raw clay soil. The presence of lanthanum (La3d) at the peak of 845.5 eV confirmed its successful binding to the clay surface (Zhang et al. 2016) (Fig. 4b). The peak at 685 eV confirms the presence of fluoride on LMC (Fig. 4c), while the peak of the O1s element continued to shift toward a less energy side of 1.9 eV differentiated with that of LMC. The binding energy of lanthanum was altered from 845.5 to 866.14 eV after interaction with fluoride. This may be due to the adsorption of fluoride on the LMC.

Batch adsorption studies

Influence of adsorbent dose

The adsorption study was conducted with different amounts of raw clay soil and LMC (1–6 g/L) to determine the effect of fluoride uptake. Adsorption of fluoride did not occur on raw clay soil, therefore, LMC was used to perform these adsorption studies. The results confirmed an increase in the adsorption of fluoride, as shown in Fig. 5a. The fluoride uptake was found to be 42.6% and 84% at the doses of 1 g/L and 3 g/L, respectively. At the doses of 4 g/L and 5 g/L, the removal rates were 95.5% and 98.3%, respectively. Upon further increasing the dose to 6 g/L, a similar result of 98.6% was obtained. The adsorption capacity of LMC was 4.26 mg/g and 1.96 mg/g at the doses of 1 g/L and 5 g/L, respectively. After the saturation of the active sites of LMC, fluoride uptake did not increase. Therefore, a 5 g/L dose of LMC was selected for further experiments.
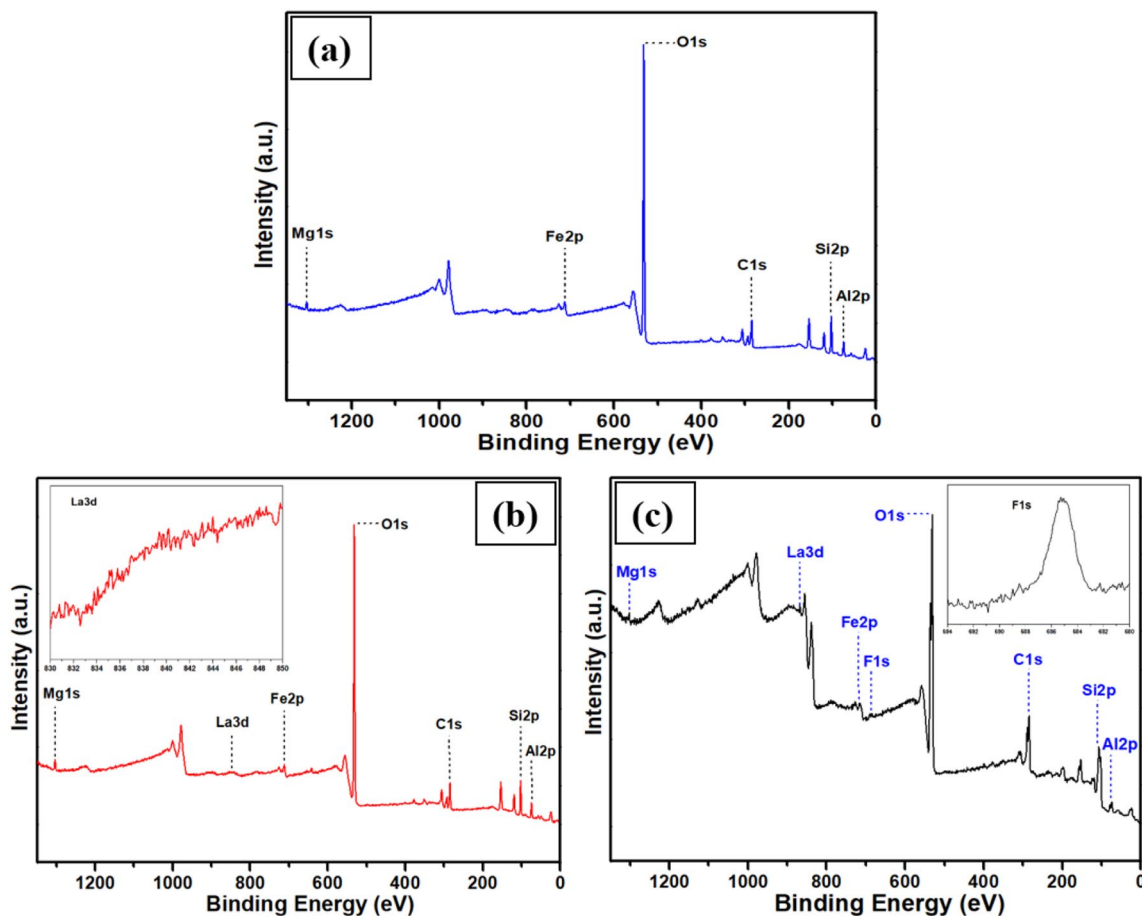
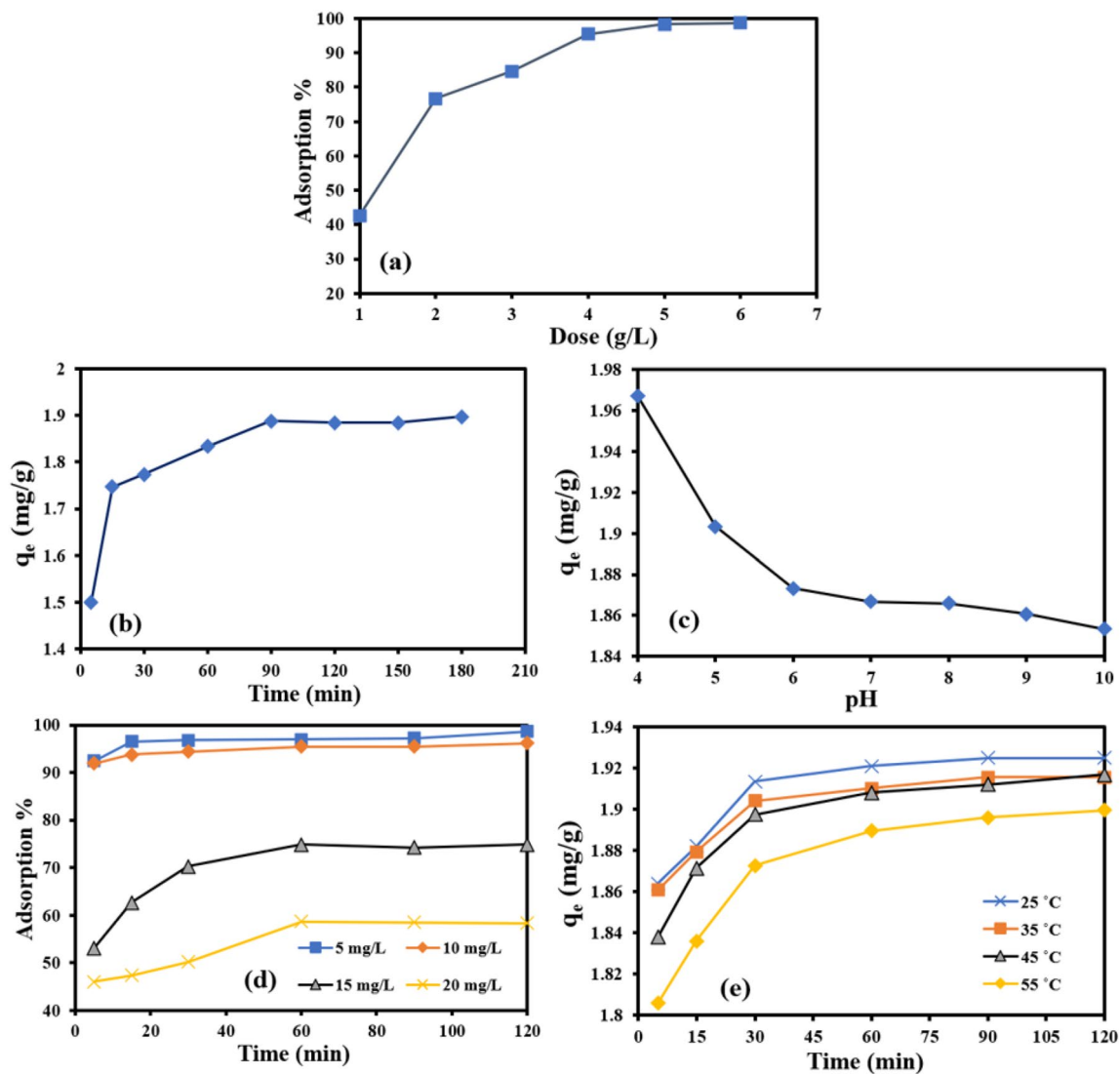**Fig. 4** X-ray photoelectron spectroscopy of raw clay soil (**a**), LMC (**b**), and after fluoride adsorption

Fig. 5 Effect of dose (**a**), effect of contact time (**b**), effect of pH (**c**), effect of starting concentration (**d**), and effect of temperature (**e**)

Effect of pH on adsorption

The ionic condition of the solution and the ionic charges on the adsorbent and adsorbate influence the fluoride uptake. The experiment for the pH effect was conducted under varying pH (4–10) of the solution. The results revealed that the fluoride uptake decreased as the pH of the solution increased, as shown in Fig. 5c. At pH 4 and pH 6, the removal rates were 98.3% and 93.6%, respectively; at neutral pH, the removal rate was 93.3%. At pH 8 and pH 10, the removal rates were 93% and 92.6%, respectively. The adsorption capacity at pH 7 was 1.86 mg/g. The decline in fluoride uptake at higher pH may result from the repulsive force between hydroxyl ions and fluoride ions as well as the decreasing positive charge on the adsorbent surface due to the increasing pH of the solution. The pHzpc of adsorbent

and pH of the solution also affect the adsorption activity, at a pH below pHzpc contains positively charge that is responsible for fluoride ions attraction, while pH above pHzpc carries a more negative charge that decreases the fluoride ions adsorption.

Effect of contact time

Time is a major factor in the adsorption process. The contact time study was carried out at different times (5–120 min), with an adsorbate concentration of 10 mg/L, at neutral pH, and at room temperature. Initially, fluoride uptake increased as the contact time increased. After achieving an equilibrium time of 60 min, fluoride uptake was constant, because the adsorbent surface had more adsorption sites at the initial stage. However, fluoride uptake did not occur after

the saturation of adsorption sites. The result revealed that adsorption efficiency was 1.5 mg/g and 1.77 mg/g at 5 min and 30 min, respectively, as shown in Fig. 5b. At an equilibrium time of 60 min, the adsorption capacity was 1.83 mg/g. The adsorption efficiency was 1.9 mg/g and 1.88 mg/g at 90 min and 120 min, respectively. After 120 min of contact time, the adsorption capacity did not increase.

Effect of fluoride concentration

The effect of fluoride concentration was evaluated by performing adsorption experiments with different concentrations of fluoride ions (5, 10, 15, and 20 mg/L), while other parameters, such as pH (7), dose (5 g/L), and temperature (25 ℃) were maintained constant. In Fig. 5d, it is obvious that, as the concentration of fluoride ions increased, the adsorption activity of fluoride decreased from 98.6 to 58.3%. The decline in the removal of fluoride might be due to an increase in the quantity of fluoride ions competing for the availability of adsorption sites in the LMC.

Effect of temperature

The influence of temperature was examined by performing adsorption studies on various warming scenarios (25 ℃, 35 ℃, 45 ℃, and 55 ℃) under optimum conditions: 5 g/L LMC dose, neutral pH, 10 mg/L initial fluoride concentration, and 0 to 120 min shaking time. The obtained results were plotted for the adsorption capacity, as shown in Fig. 5e. The adsorption capacity reached 1.92 mg/g at 25 ℃ and decreased to 1.88 mg/g at 55 ℃. Temperature affects the energy balance during adsorption and the kinetics of the adsorbed ions (Wambu and Kurui 2018). Results revealed that when the temperature increased, the adsorption capacity decreased, showing the adsorption process is exothermic.

Adsorption isotherm model

The distribution of adsorbed molecules between the solid and liquid phases at equilibrium can be determined from the adsorption isotherm data. The mechanism of fluoride adsorption can be evaluated based on the arrangement of fluoride ions that occurs monolayer or multilayer and this behavior can also be evaluated by the mathematical model. Monolayer arrangement of adsorbate on the surface of adsorbent predicts adsorption activity is chemisorption in nature, while multilayer arrangement of adsorbate determines physisorption. The expression of the model gives information about the exponential distribution of energies and adsorptive sites. Moreover, the fluoride adsorption capacity of LMC can be determined. The data generated for fluoride adsorption on LMC were used for the Freundlich, Langmuir, and Temkin isotherm models.

Langmuir isotherm model

Equilibrium studies on the fluoride adsorption on LMC were carried out at various concentrations (5–20 mg/L). The Langmuir adsorption isotherm assumes that a monolayer arrangement occurs on the adsorbent surface (Chaudhry et al. 2017). The equation for this model is represented by the following equation:

$$C_e/q_e = \frac{1}{Q_0 b} + \frac{C_e}{Q_0}. \tag{7}$$

Figure 6a shows a plot of the Langmuir isotherm C_e/q_e (specific adsorption) versus C_e (equilibrium concentration). Q_0 (mg/g) and b (L/mg) are the Langmuir constants, which represent the maximum adsorption capacity and the rate of adsorption, respectively. The values of these constants were determined by the slope and intercept of the plot and are presented in Table 1.

The dimensionless separation factor for Langmuir isotherm is expressed as follows:

$$R_L = \frac{1}{\left(1 + bC_0\right)}, \tag{8}$$

where C_0 is the initial fluoride concentration (mg/L) and b is a constant for the adsorption equilibrium (L/mg) of Langmuir. R_L is a separation factor that confirms the behavior of adsorption; in particular, $0<R_L<1$ indicates favorable adsorption, whereas $R_L>1$ indicates unfavorable adsorption. In our study, $R_L<1$; therefore, fluoride adsorption on the LMC was favorable (Gautam et al. 2018).

Freundlich isotherm model

The Freundlich isotherm assumes that the formation of a heterogeneous layer occurs during adsorption. The equation for this adsorption model is expressed as follows:

$$\ln qe = \ln K_f - \frac{1}{n}\ln Ce, \tag{9}$$

where C_e, q_e, and K_f denote the concentration of fluoride (mg/L) at equilibrium, amount of the adsorbed fluoride (mg/g), and capacity (mg/g(L/mg)$^{1/n}$) of LMC for fluoride uptake, respectively. The plot of $\ln q_e$ versus $\ln C_e$ for the uptake of fluoride on LMC yielded a straight line with a correlation coefficient, and n is an equilibrium constant of the Freundlich isotherm (Fig. S.3a). It is assumed that the adsorption capacity increases as K_f increases. The value of n is used to check the degree of nonlinearity whether the adsorption is linear ($n = 1$), chemical phenomena ($n > 1$), and physical phenomena ($n < 1$). In this adsorption study, $n > 1$ (Table 1).
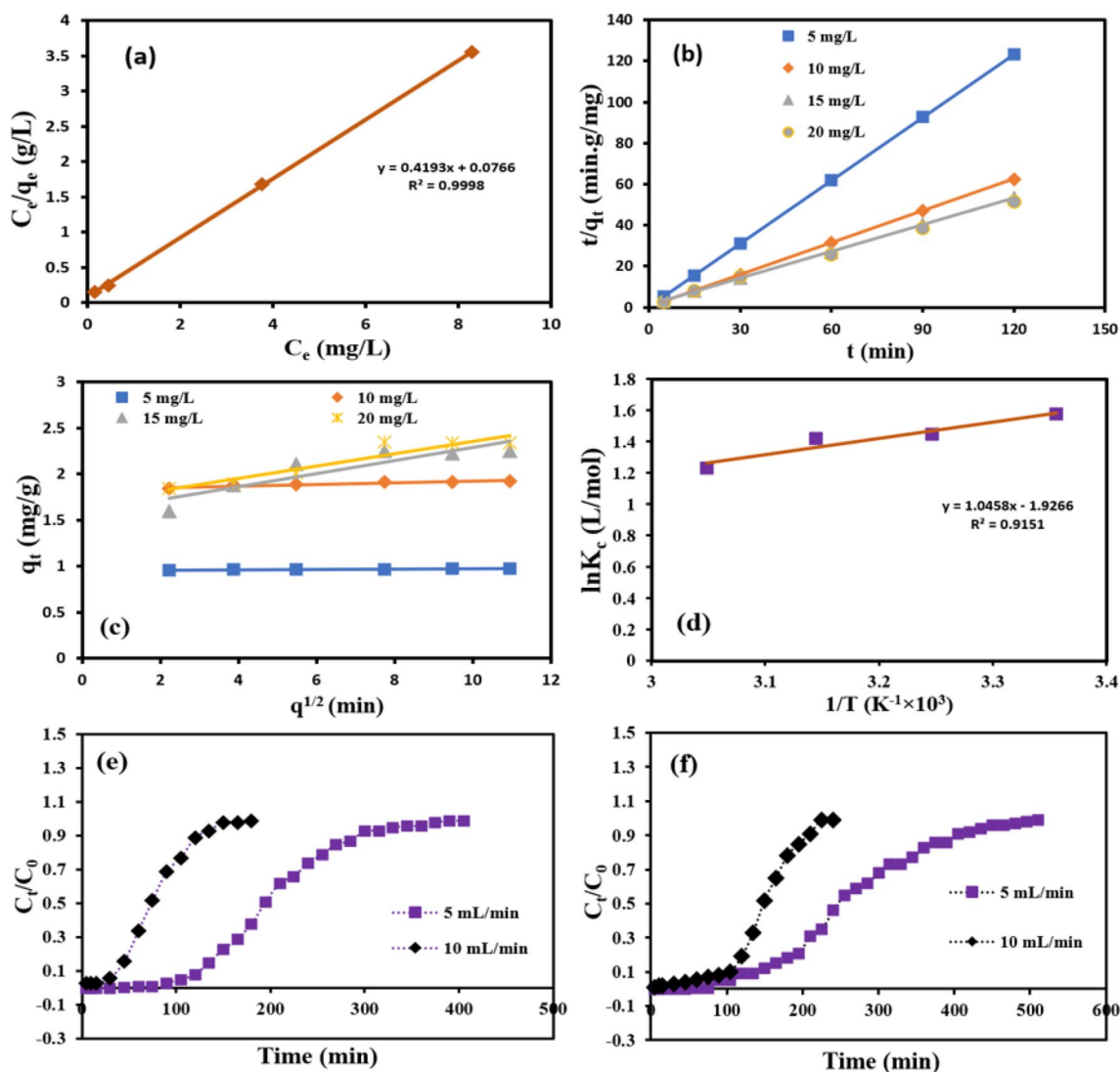
Fig. 6 Plot of Langmuir model (**a**), pseudo-second-order kinetics (**b**), intraparticle diffusion (**c**), thermodynamic plot (**d**), breakthrough curve of 3 cm (**e**), and breakthrough curve of 6 cm (**f**)

Table 1 Values of parameters related adsorption isotherms

Langmuir isotherm				Freundlich isotherm			Temkin isotherm		
Q_0 (mg/g)	b (L/mg)	R_L	R^2	K_F (mg/g(L/mg)$^{1/n}$)	n	R^2	B	K_T(e^c/B)	R^2
2.384	0.0321	0.861	0.998	1.704	5.202	0.758	0.306	369.24	0.825

Temkin isotherm model

The Temkin isotherm model characterized the uniform dispersal of binding energies on the adsorbent surface. Sorbate–sorbent interactions decrease the adsorption heat as surface coverage increases during adsorption (Ayawei et al. 2017).

$$q_e = B\ln K_T + B\ln C_e, \tag{10}$$

where K_T is the Temkin isotherm constant (L/g), B is a constant (RT/bT) for the heat of sorption (J/mol), and R is the gas constant (8.314 J/mol K). The values of B and K_T obtained from the intercept and slope of the plot of q_e versus $\ln C_e$ (Fig. S.3b), and the values of these parameters are listed in Table 1.

The parameters of the adsorption isotherm models revealed that the regression coefficient R^2 value was 0.998 for the Langmuir model, which was comparatively higher than 0.758 for the Freundlich model and 0.825 for the Temkin model. The

Table 2 Values of kinetics and intraparticle diffusion model parameters of fluoride adsorption

C_0 (mg/L)	Pseudo-first-order kinetic			Pseudo-second-order kinetic			Intraparticle diffusion model		
	q_e (mg/g)	K_1	R^2	q_e (mg/g)	K_2	R^2	Ki (m)	C	R^2
5	0.018	0.0143	0.964	0.974	6.620	1	0.001	0.956	0.841
10	0.080	0.0087	0.933	1.926	1.176	1	0.008	1.832	0.903
15	0.644	0.0074	0.975	2.298	0.170	0.999	0.070	1.581	0.806
20	0.790	0.0073	0.986	2.415	0.124	0.998	0.067	0.886	0.886

values of b and Q_0 for Langmuir were 0.032 and 2.384 mg/g, respectively. The Langmuir equation was best fitted for the adsorption of fluoride on LMC.

Kinetic studies

The adsorption rate of fluoride ions on the LMC surface was evaluated using kinetic studies. The adsorption dynamics were elaborated by pseudo-first-order kinetics as expressed in Eq. 11, and pseudo-second-order kinetics, as expressed in Eq. 12, to determine the rate of fluoride adsorption on LMC.

$$\log(q_e - q_t) = \log q_e \left(\frac{k_1}{2.303} \right) t, \tag{11}$$

$$t/q_e = \frac{1}{(k_2 q_e 2)} + (1/q_e)t, \tag{12}$$

where q_t is the quantity of fluoride (mg/g) adsorbed on the LMC at any time (t), k_1 is the adsorption rate constant (1/min) of first-order kinetics, and k_2 is the adsorption rate constant (mg/g min) of second-order kinetics. The equilibrium adsorption capacity and constants were obtained by plotting $\log(q_e - q_t)$ against t (Fig. S3c). A plot of pseudo-second-order kinetics is shown in Fig. 6b. The kinetic data showed that the R^2 value was 1 for fluoride adsorption on LMC; therefore, the pseudo-second-order reaction was more suitable. The parameters of both kinetics are listed in Table 2.

Intraparticle diffusion (IPD) model

The IPD model infers the mechanistic approach of adsorbate transfer and transport from the solid–liquid interface onto the solid adsorbent. It assumes that information about the boundary layer thickness can be obtained by the intercept. A higher intercept indicates a greater contribution of adsorption on the surface in the rate-determining step (Sahu et al. 2020a, b). The equation for the IPD model is given by Weber–Morris as follows:

$$q_t = kt^{1/2} + C, \tag{13}$$

Table 3 Thermodynamic parameters of fluoride adsorption onto the LMC

Temperature (K)	Thermodynamic parameters		
	ΔG^O (kJ/mol)	ΔH^O (kJ/mol)	ΔS^O (J/mol K)
298 K	4.764	− 8.694	− 16.017
308 K	4.924		
318 K	5.084		
328 K	5.245		

where k denotes the rate constant (mg/(g min$^{0.5}$)) of the IPD model and C is a constant (mg/g) for the boundary layer thickness. Figure 6c shows that the linear graph does not cross the starting point, which confirms that IPD is not only ascribed to the rate controlling for fluoride adsorption on the LMC. The parameters of the IPD model are listed in Table 2.

Thermodynamic studies of fluoride adsorption on LMC

The thermodynamic parameters, such as the change in entropy (ΔS), Gibbs free energy (ΔG), and enthalpy (ΔH), during the adsorption of fluoride on LMC were confirmed by thermodynamic studies. These parameters can be evaluated at various temperatures (25 ℃, 35 ℃, 45 ℃, and 55 ℃) using the following equations:

$$K_c = q_e/C_e, \tag{14}$$

$$\ln K_c = (\Delta S/R) - (\Delta H/RT), \tag{15}$$

$$\Delta G° = -RT \ln K_c, \tag{16}$$

where K_c (L/g) denotes the standard thermodynamic constant, T is the temperature in Kelvin, and R is the universal gas constant (8.314 J/mol K). The changes in enthalpy and entropy can be determined by plotting $\ln Kc$ against $1/T$ (Saikia et al. 2017). In this study, adsorption was exothermic owing to the negative value of ΔH (Table 3). The positive value of the ΔG indicates that the process was non-spontaneous, and the negative value of entropy point out a decrease

Table 4 Values of different fixed bed and Thomas model parameters

Column parameters								Thomas parameters		
C_o (mg L^{-1})	Z (cm)	Q (mL min^{-1})	t_{total} (min)	m_{total} (mg)	q_{total} (mg)	q_e (mg/g)	V_{eff} (mL)	K_{TH} (mL min^{-1} mg^{-1})	Q_o (mg g^{-1})	R^2
10	3	5	405	20.25	20.24	6.74	2025	0.0033	3799.44	0.925
10	3	10	180	18.00	17.46	5.82	1800	0.0048	2643.71	0.991
10	6	5	510	25.50	25.49	4.24	2550	0.0014	1764.96	0.909
10	6	10	240	24.00	23.76	3.96	2400	0.0034	1349.26	0.950

in randomness at the LMC surface during the adsorption process. The thermodynamic plot is shown in Fig. 6d.

Continuous adsorption study

Effect of fixed bed depth

The continued adsorption study was conducted with two different bed heights (3 cm and 6 cm) and two flow rates for each bed depth to check the effect of fluoride adsorption in a column. The starting concentration of the influent was 10 mg/L. The obtained breakthrough curves for both bed depths are shown in Fig. 6e, f. Data from the column study showed that, as the bed length increased from 3 to 6 cm, the saturation time increased from 390 to 480 min, and the processed effluent increased from 2025 to 2400 mL with a flow rate of 5 mL/min. The saturation time for a flow rate of 10 mL/min increased from 180 to 225 min (Table 4). The breakthrough time increased because of the increasing amount of LMC, which provided more adsorption sites for the adsorption of fluoride.

Effect of solution flow rate

The effect of influent flow rate on the breakthrough curve and saturation time was observed at two different flow rates, 5 mL/min and 10 mL/min. It was observed that breakthrough generally occurred rapidly with a higher flow rate, and the column was exhausted in less time. As the flow rate increased, the saturation time decreases. At 5 mL/min, the exhaustion of the column slowed down because of the longer contact time. This means that the adsorption of fluoride increased as the flow rate decreased. This is due to the longer interaction time between the fluoride ions and LMC surface.

Thomas model

The Thomas model was employed to evaluate the maximum adsorption capacity of the LMC in a column. This model was extensively applied to evaluate column performance. The equation of the Thomas model is expressed as follows:

$$\ln\left(\frac{C_0}{C_t} - 1\right) = \frac{k_{TH}q_e m}{Q} - k_{TH}C_0 t, \tag{17}$$

where k_{TH} is the rate constant (mL/min•mg) of the Thomas model, q_e is the adsorption capacity (mg/g) at equilibrium, Q is the flow rate (mL/min) of the solution, and m is the amount of LMC in the column. A plot of the Thomas model is shown in Fig. S4a, b, and the values of the Thomas parameters are listed in Table 4.

Adams–Bohart model

The Adams–Bohart model describes that the rate of adsorption is proportional to the fluoride concentration and the remaining capacity of the LMC. This model is used for the elaboration of the starting portion of the breakthrough curve during continuous adsorption in the column, and the equation is presented below.

$$\text{n}\left(\frac{C_t}{C_0}\right) = K_{AB}N_0\frac{z}{U_0} - K_{AB}C_0 i \tag{18}$$

where K_{AB} denotes the Adams–Bohart rate constant for adsorption, N_0 is the maximum adsorption capacity (mg/L) per unit dose of LMC used in the column, z is the bed depth (cm) of the adsorbent, and U_0 is the linear velocity (cm/min) of the influent solution. The plot for Adams–Bohart is shown in Fig. S4c, d. The values of the different parameters of this model are presented in Table S1.

Yoon–Nelson model

The Yoon–Nelson model was used to evaluate the breakthrough behavior of fluoride on the LMC in the column. The expression of this model is given by the following equation (Djelloul and Hamdaoui 2015):

$$\ln\left(\frac{C_t}{C_0 - C_t}\right) = \tau k_{YN} - k_{YN}t, \tag{19}$$

where k_{YN} is the rate constant (L/min) of Yoon–Nelson, and τ is the time required for 50% adsorbate breakthrough.

The values of k_{YN} and τ were obtained from the plots of $\ln[(C_t/C_0 - C_t)]$ against t for different flow rates (Table S1). The plot for this model is shown in Fig. S5a, b.

Clark model

This model was used to evaluate mass transfer using the Freundlich isotherm (Saadi et al. 2013). The linear equation is expressed as follows:

$$\ln\left[\left(\frac{C_0}{C}\right)^{n-1} - 1\right] = \ln A - rt, \tag{20}$$

where n is the Freundlich parameter, and C_0 and C are the influent and effluent concentrations (mg/L), respectively. A and r (1/h) are constants for the Clark model. The plot of $\ln[(C_0/C)^{n-1} - 1]$ versus time is shown in Fig. S5c, d. The values of A and r can be obtained from the slope and intercept of the plot, respectively.

The performance of the column was evaluated by applying the Adams–Bohart, Clark, Yoon–Nelson, and Thomas models. The Thomas model revealed that the value of K_{TH} increased as the flow rate for both bed depths increased, whereas the value of q_0 decreased, as shown in Table 4. This effect occurred because of the driving force between the fluoride ions and the LMC surface. Column data according to the Adams–Bohart equation indicated that the adsorption capacity (N_0) and rate constant (K_{AB}) decreased as the bed height of LMC increased (Table S1). The time needed for adsorbate breakthrough (τ) decreased as the bed depth increased, and the rate constant (K_{YN}) of Yoon–Nelson increased as the flow rate increased from 5 to 10 mL/min, while Clark constant (A) also decreased (Table S1 and Table S2).

Reusability test of LMC

The reusability of LMC was determined by adsorption and desorption processes. A predetermined amount of LMC was mixed in a 10 mg/L solution of fluoride and was shaken in an orbital shaker for 2 h. The desorption of the fluoride ions from the LMC surface was compared using two different solutions of 0.1 M NaOH and 0.1 M NaHCO$_3$, and the mixture was shaken in an orbital shaker for 6 h. Afterward, the adsorbent was separated and cleaned two to three times with distilled water. The dried LMC was further used for the adsorption of fluoride, and the competitive concentration was checked using a selective ion electrode. The same procedure was followed for each cycle. The adsorbent was successfully applied for four adsorption cycles. The adsorption capacity (1.94 mg/g) of the adsorbent was decreased from the first cycle to the fourth cycle (0.34 mg/g) with NaOH solution. The maximum adsorption was 97% for the first cycle and 17% for the fourth
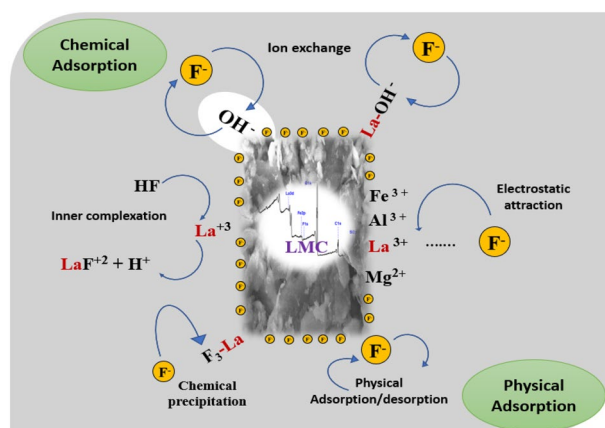

**Fig. 7** Probable mechanism of fluoride adsorption on LMC

cycle, while, adsorption percentage was obtained 19% and 10% with NaHCO$_3$ solution as shown in Fig. 8a. Regeneration using NaHCO$_3$ shows lower adsorption of fluoride compared to regeneration using NaOH, because NaOH is a strong base that desorbed more fluoride ions in each regeneration cycle from the surface of LMC.

Mechanism of fluoride adsorption on LMC

The mechanism of fluoride adsorption on LMC is illustrated in Fig. 7. This mechanism is described based on available adsorption sites and cations on the LMC as well as their interactions with fluoride ions. Ligand exchange occurs between fluoride ions and metallic cations (La^{3+}, Al^{3+}, Mg^{2+}, and Fe^{3+}) owing to the isoelectronic and ionic radii of the fluoride ions and OH$^-$ (Sengupta et al. 2020). The electrostatic attraction was found between positively charged lanthanum ions and negatively charged fluoride ions. pHzpc of the adsorbent also influences the adsorption of fluoride. When the pH is lower than the pHzpc, the adsorbent surface carries a more positive charge then it interacts with fluoride ions and occurs more adsorption. While in the case of pH more than pHzpc, less positive charge and more OH$^-$ ion that opposes the fluoride adsorption on the LMC. The presence of lanthanum on the surface of the clay soil was confirmed in the XPS data (Sahu et al. 2020a, b). As the pH of the solution increased, the protonation of M–OH formed M–OH$_2^+$, which facilitated the binding of fluoride ions. The F1s peak of 685 eV confirmed the successful attachment of F$^-$ to the LMC surface.

Effect of competitive ions

During the adsorption process, the other ions that are available in the solution affect the adsorption of the target adsorbate. The effects of chloride, nitrate, sulfate, and bicarbonate ions on fluoride adsorption were evaluated. A
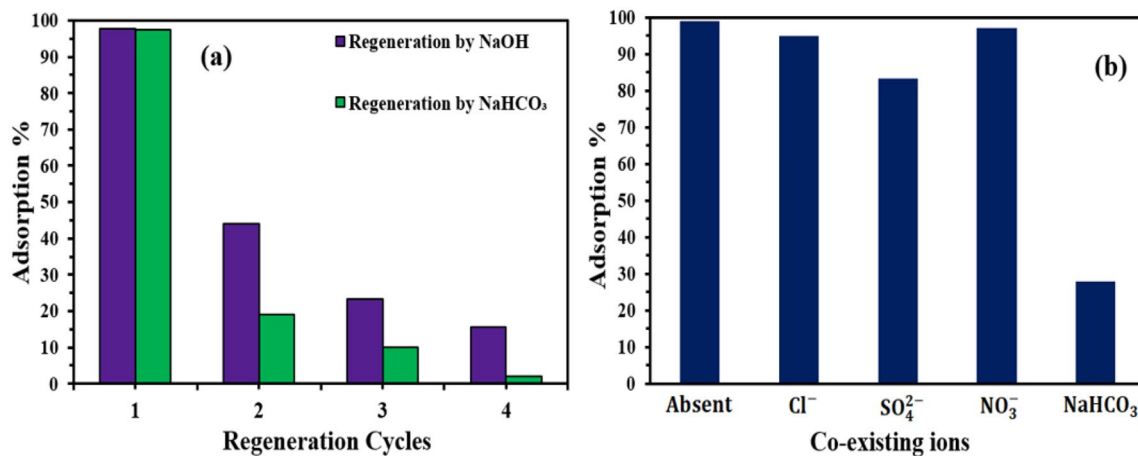
Fig. 8 Regeneration study of LMC (**a**) and effect of competitive ions on fluoride adsorption (**b**)

Table 5 Comparison of adsorption capacity of LMC with different adsorbents

S.N.	Adsorbent	pH	Adsorption capacity (mg/g)	References
1.	Lanthanum and Aluminum modified clay	6	1.3	Zhang et al. (2016)
2.	Lateritic soil	6	0.5	Iriel et al. (2018)
3.	Manganese modified bentonite	4	2.4	Mudzielwana et al. (2018)
4.	Mechanochemically activated clay soil	6	1.87	Obijole et al. (2019)
5.	Natural clay (Kaolinite)	5.8	0.448	Nabbou et al. (2019)
6.	Kaolin-Bentonite composites	6.5	0.3	Annan et al. (2021)
7.	Lanthanum-modified pond clay soil	7	1.96	Present study

combined solution of individual ions with fluoride concentrations of 250 and 10 mg/L was used in this study. As shown in Fig. 8b, the observations confirmed that chloride and nitrate ions did not alter the fluoride ion capacity, whereas the presence of bicarbonate and sulfate showed a negative influence. The presence of sulfate ions caused the adsorption percentage to decrease from 98 to 83%, while the presence of bicarbonate ions caused the adsorption percentage to decrease from 98 to 35%. This decline in fluoride adsorption might be a result of the ionic repulsive force between fluoride ions and sulfate/bicarbonate ions that alters the interaction of fluoride with adsorption sites available on the LMC surface.

Comparison of adsorption capacity of LMC with different adsorbents

The adsorption capacity of LMC was compared with that of different types of clay-based adsorbents for fluoride adsorption. It was found that LMC had a better adsorption capacity than previously reported adsorbents, as presented in Table 5.

Application of LMC for groundwater treatment

The developed adsorbent was examined for its suitability to treat real groundwater. Fluoride-containing water samples were collected from different locations in the village Chouhatta (25°57′08″ N, 80°57′13″ S). First, analysis of fluoride, pH, and TDS was tested in the collected sample, and the concentration of fluoride was found 5.6 mg/L (village hand pump) and 3.9 mg/L (school hand pump). A total of 0.5 g LMC was added to a 100 mL groundwater sample and shaken for 60 min at room temperature. After the treatment of the groundwater sample, fluoride ions were significantly removed. Fluoride ions reached 1.4 mg/L from 3.9 mg/L in school hand pump water, which is below the permissible limit set for drinking purposes. The analyzed groundwater parameters are listed in Table 6.

Conclusions

In the present work, a composite of clay and lanthanum was successfully developed and applied for fluoride removal by batch and continuous flow processes in a

Table 6 Groundwater analysis results for LMC adsorbent

Parameters	Chouhatta, hand pump water	After adsorption	School, hand pump water	After adsorption
Fluoride (mg/L)	5.6	2.1	3.9	1.4
pH	7.9	7.5	7.7	7.4
Na^+ (mg/L)	530.7	488.3	508.3	453.6
K^+ (mg/L)	12.6	8.5	14.2	9.4
TDS (mg/L)	552.7	520.3	467.4	435

column. The highest adsorption of fluoride ions on LMC was 97% with an adsorption capacity of 1.96 mg/g. Column adsorption studies were performed using two different adsorbent bed depths in a column. As the bed height increased, the adsorption capacity and efficiency of the column increased. Moreover, as the flow rate of the solution increased, the adsorption of fluoride decreased. The Thomas model was best fitted for column data in comparison with Adams–Bohart, Yoon–Nelson, and Clark models. The pseudo-second-order kinetics and Freundlich adsorption isotherms fitted well for fluoride adsorption on the LMC. The exchange of legends between the present metallic cations and fluoride ions as well as the electrostatic force between the positively charged hydroxyl group and fluoride were responsible for the chemisorption mechanism. The protonation of M–OH produced $M–OH_2^+$, which attracted fluoride ions. The presence of sulfate and bicarbonate ions in the aqueous solution had negative results for fluoride adsorption. The LMC test for groundwater treatment had significant results, with a fluoride concentration of 1.4 mg/L from 3.9 mg/L. Based on the results of this adsorption study, LMC could be a good candidate for the defluorination of contaminated groundwater. A large amount of adsorbent preparation from locally available clay soil can be used in filter systems and will provide fluoride-free drinking water to the villages community.

Declarations

References

Adeyemo AA, Adeoye IO, Bello OS (2017) Adsorption of dyes using different types of clay: a review. Appl Water Sci 7(2):543–568. https://doi.org/10.1007/s13201-015-0322-y

Adimalla N, Venkatayogi S, Das SVG (2019) Assessment of fluoride contamination and distribution: a case study from a rural part of Andhra Pradesh. India Appl Water Sci 9(4):1–15. https://doi.org/10.1007/s13201-019-0968-y

Akafu T, Chimdi A, Gomoro K (2019) Removal of fluoride from drinking water by sorption using diatomite modified with aluminum hydroxide. J Anal Methods Chem 2019:1–11. https://doi.org/10.1155/2019/4831926

Annan E, Nyankson E, Agyei-Tuffour B et al (2021) Synthesis and characterization of modified kaolin-bentonite composites for enhanced fluoride removal from drinking water. Adv Mater Sci Eng 2021:1–12. https://doi.org/10.1155/2021/6679422

Atasoy AD, Yesilnacar MI, Sahin MO (2013) Removal of fluoride from contaminated ground water using raw and modified bauxite. Bull Environ Contam Toxicol 91(5):595–599. https://doi.org/10.1007/s00128-013-1099-z

Ayalew AA (2020) Development of kaolin clay as a cost-effective technology for defluoridation of groundwater. Int J Chem Eng 2020:1–10. https://doi.org/10.1155/2020/8820727

Ayawei N, Ebelegi AN, Wankasi D (2017) Modelling and interpretation of adsorption isotherms. J Chem 2017:1–11. https://doi.org/10.1155/2017/3039817

Bharti VK, Giri A, Kumar K (2017) Fluoride sources, toxicity and its amelioration: a review. Peertechz J Environ Sci Toxicol 2(1):021–032. https://doi.org/10.17352/aest.000009

Blott SJ, Pye K (2001) GRADISTAT: a grain size distribution and statistics package for the analysis of unconsolidated sediments.

Earth Surf Process Landf 26(11):1237–1248. https://doi.org/10.1002/esp.261

Bukalo NN, Ekosse GIE, Odiyo JO, Ogola JS (2017) Fourier transform infrared spectroscopy of clay size fraction of cretaceous-tertiary kaolins in the Douala sub-basin, Cameroon. Open Geosci 9(1):407–418. https://doi.org/10.1515/geo-2017-0031

Caponi N, Collazzo GC, Jahn SL, Dotto GL, Mazutti MA, Foletto EL (2017) Use of Brazilian kaolin as a potential low-cost adsorbent for the removal of malachite green from colored effluents. Mater Res 20:14–22. https://doi.org/10.1590/1980-5373-MR-2016-0673

Castro LFD, Brandão VS, Bertolino LC, de Souza WF, Teixeira VG (2019) Phosphate adsorption by montmorillonites modified with lanthanum/iron and a laboratory test using water from the Jacarepaguá Lagoon (RJ, Brazil). J Braz Chem Soc 30(3):641–657. https://doi.org/10.21577/0103-5053.20180236

Chaudhry SA, Zaidi Z, Siddiqui SI (2017) Isotherm, kinetic and thermodynamics of arsenic adsorption onto Iron-zirconium binary oxide-coated sand (IZBOCS): modelling and process optimization. J Mol Liq 229:230–240. https://doi.org/10.1016/j.molliq.2016.12.048

Corral-Capulin NG, Vilchis-Nestor AR, Gutiérrez-Segura E, Solache-Rios M (2019) Comparison of the removal behavior of fluoride by Fe^{3+} modified geomaterials from water. Appl Clay Sci 173:19–28. https://doi.org/10.1016/j.clay.2019.03.003

Dessalegne M, Zewge F, Mammo W, Woldetinsae G, Diaz I (2018) Effective fluoride adsorption by aluminum oxide modified clays: Ethiopian bentonite vs commercial montmorillonite. Bull Chem Soc Ethiop 32(2):199–211. https://doi.org/10.4314/bcse.v32i2.2

Dewage NB, Liyanage AS, Pittman CU Jr, Mohan D, Mlsna T (2018) Fast nitrate and fluoride adsorption and magnetic separation from water on α-Fe_2O_3 and Fe_3O_4 dispersed on Douglas fir biochar. Bioresour Technol 263:258–265. https://doi.org/10.1016/j.biortech.2018.05.001

Djelloul C, Hamdaoui O (2015) Dynamic adsorption of methylene blue by melon peel in fixed-bed columns. Desalin Water Treat 56(11):2966–2975. https://doi.org/10.1080/19443994.2014.963158

Elgamouz A, Tijani N, Shehadi I, Hasan K, Kawam MAF (2019) Characterization of the firing behaviour of an illite-kaolinite clay mineral and its potential use as membrane support. Heliyon 8(2019):1–9. https://doi.org/10.1016/j.heliyon.2019.e02281

Enalou HB, Moore F, Keshavarzi B, Zarei M (2018) Source apportionment and health risk assessment of fluoride is water resources, south of Fars province, Iran: stable isotopes ($\delta18O$ & δD) and geochemical modeling approaches. Appl Geochem 98:197–205. https://doi.org/10.1016/j.apgeochem.2018.09.019

Fito J, Said H, Feleke S, Worku A (2019) Fluoride removal from aqueous solution onto activated carbon of Catha edulis through the adsorption treatment technology. Environ Sys Res 8(1):1–10. https://doi.org/10.1186/s40068-019-0153-1

Garcia-Sanchez JJ, Solache-Rios M, Martinez-Gutierrez JM, Arteaga-Larios NV, Ojeda-Escamilla MC, Rodriguez-Torres I (2016) Modified natural magnetite with Al and La ions for the adsorption of fluoride ions from aqueous solutions. J Fluor Chem 186:115–124. https://doi.org/10.1016/j.jfluchem.2016.05.004

Gautam A, Rawat S, Verma L, Singh J, Sikarwar S, Yadav BC, Kalamdhad AS (2018) Green synthesis of iron nanoparticle from extract of waste tea: an application for phenol red removal from aqueous solution. Environ Nanotechnol Monit Manag 10:377–387. https://doi.org/10.1016/j.enmm.2018.08.003

Ghosal PS, Gupta AK, Ayoob S (2015) Effect of formation pH, molar ratio and calcination temperature on the synthesis of an anionic clay based adsorbent targeting defluoridation. Appl Clay Sci 116:120–128. https://doi.org/10.1016/j.clay.2015.08.026

Hanse A, Chabukdhara M, Baruah SG, Boruah H, Gupta SK (2019) Fluoride contamination in groundwater and associated health risks in Karbi Anglong District, Assam, Northeast India. Environ Monit Assess 191(12):1–17. https://doi.org/10.1007/s10661-019-7970-6

Iriel A, Bruneel SP, Schenone N, Cirelli AF (2018) The removal of fluoride from aqueous solution by a lateritic soil adsorption: kinetic and equilibrium studies. Ecotoxicol Environ Saf 149:166–172. https://doi.org/10.1016/j.ecoenv.2017.11.016

Jagtap S, Yenkie MK, Labhsetwar N, Rayalu S (2012) Fluoride in drinking water and defluoridation of water. Chem Rev 112(4):2454–2466. https://doi.org/10.1021/cr2002855

Kadam A, Wagh V, Umrikar B, Sankhua R (2020) An implication of boron and fluoride contamination and its exposure risk in groundwater resources in semi-arid region, western India. Environ Dev Sustain 22(7):7033–7056. https://doi.org/10.1007/s10668-019-00527-w

Karunanidhi D, Aravinthasamy P, Subramani T, Roy PD, Srinivasamoorthy K (2019) Risk of fluoride-rich groundwater on human health: remediation through managed aquifer recharge in a hard rock terrain South India. Nat Resour Res 29(4):1–27. https://doi.org/10.1007/s11053-019-09592-4

Kofa GP, Gomdje VH, Telegang C, Koungou SN (2017) Removal of fluoride from water by adsorption onto fired clay pots: kinetics and equilibrium studies. J Appl Chem 2017:1–7. https://doi.org/10.1155/2017/6254683

Lambert JF (2018) Organic pollutant adsorption on clay minerals. In: Bergaya F (ed) Developments in clay science. Elsevier, Amsterdam, pp 195–253. https://doi.org/10.1016/B978-0-08-102432-4.00007-X

Liu R, Mei X, Zhang J, Zhao DB (2019) Characteristics of clay minerals in sediments of Hemudu area, Zhejiang, China in Holocene and their environmental significance. China Geol 2(1):8–15. https://doi.org/10.31035/cg2018069

Ma Z, Zhang Q, Weng X, Mang C, Si L, Guan Z, Cheng L (2018) Fluoride ion adsorption from wastewater using magnesium (II), aluminum (III) and titanium (IV) modified natural zeolite: kinetics, thermodynamics, and mechanistic aspects of adsorption. J Water Reuse Desalin 8(4):479–489. https://doi.org/10.2166/wrd.2017.037

Madejova J, Gates WP, Petit S (2017) IR spectra of clay minerals. Dev Clay Sci 8:107–149. https://doi.org/10.1016/B978-0-08-100355-8.00005-9

Majewska-Nowak K, Grzegorzek M, Kabsch-Korbutowicz MAŁGORZATA (2015) Removal of fluoride ions by batch electrodialysis. Environ Prot Eng 41(1):67–81. https://doi.org/10.5277/epe150106

Mei L, Qiao H, Ke F et al (2020) One-step synthesis of zirconium dioxide-biochar derived from Camellia oleifera seed shell with enhanced removal capacity for fluoride from water. Appl Surf Sci 509:144685. https://doi.org/10.1016/j.apsusc.2019.144685

Mobarak M, Selim AQ, Mohamed EA, Seliem MK (2018) Modification of organic matter-rich clay by a solution of cationic surfactant/H_2O_2: a new product for fluoride adsorption from solutions. J Clean Prod 192:712–721. https://doi.org/10.1016/j.jclepro.2018.05.044

Mudzielwana R, Gitari MW, Akinyemi SA, Msagati TA (2018) Performance of Mn^{2+}-modified bentonite clay for the removal of fluoride from aqueous solution. S Afr J Chem 71:15–23. https://doi.org/10.17159/0379-4350/2018/v71a2

Mukherjee I, Singh UK (2018) Groundwater fluoride contamination, probable release, and containment mechanisms: a review on Indian context. Environ Geochem Health 40(6):2259–2301. https://doi.org/10.1007/s10653-018-0096-x

Mukherjee I, Singh UK (2020) Fluoride abundance and their release mechanisms in ground water along with associated human health

risks in a geologically heterogeneous semi-arid region of east India. Microchem J. https://doi.org/10.1016/j.microc.2019.104304

Mumtaz N, Pandey G, Labhasetwar PK (2015) Global fluoride occurrence, available technologies for fluoride removal and electrolytic defluoridation: a review. Crit Rev Environ Sci Technol 45(21):2357–2389. https://doi.org/10.1080/10643389.2015.1046768

Nabbou N, Belhachemi M, Boumelik M et al (2019) Removal of fluoride from groundwater using natural clay (kaolinite): optimization of adsorption conditions. C R Chim 22(2–3):105–112. https://doi.org/10.1016/j.crci.2018.09.010

Nagaraj A, Sadasivuni KK, Rajan M (2017) Investigation of lanthanum impregnated cellulose, derived from biomass, as an adsorbent for the removal of fluoride from drinking water. Carbohydr Polym 176:402–410. https://doi.org/10.1016/j.carbpol.2017.08.089

Nagaraj A, Pillay K, Kumar SK, Rajan M (2020) Dicarboxylic acid cross-linked metal ion decorated bentonite clay and chitosan for fluoride removal studies. RSC Adv 10(28):16791–16803. https://doi.org/10.1039/D0RA00598C

Obijole OA, Gitari MW, Ndungu PG, Samie A (2019) Mechanochemically activated Aluminosilicate clay soils and their application for defluoridation and pathogen removal from groundwater. Int J Environ Res Public Health 16(4):1–19. https://doi.org/10.3390/ijerph16040654

Preethi J, Meenakshi S (2018) Fabrication of La3+ impregnated chitosan/β-cyclodextrin biopolymeric materials for effective utilization of chromate and fluoride adsorption in single systems. J Chem Eng Data 63(3):723–731. https://doi.org/10.1021/acs.jced.7b00889

Raghav S, Kumar D (2018) Adsorption equilibrium, kinetics, and thermodynamic studies of fluoride adsorbed by tetrametallic oxide adsorbent. J Chem Eng Data 63(5):1682–1697. https://doi.org/10.1021/acs.jced.8b00024

Saadi Z, Saadi R, Fazaeli R (2013) Fixed-bed adsorption dynamics of Pb (II) adsorption from aqueous solution using nanostructured γ-alumina. J Nanostructure Chem 3(1):1–8. https://doi.org/10.1186/2193-8865-3-48

Saeed KAH, Kassim KA, Yunus NZM, Nur H (2013) Characterization of hydrated lime-stabilized brown kaolin clay. Int J Eng Res Technol 2(11):3722–3727

Saeed KAH, Kassim KA, Yunus NZM, Nur H (2015) Physico-chemical characterization of lime stabilized tropical kaolin clay. Jurnal Teknologi 72(3):83–90. https://doi.org/10.11113/jt.v72.4021

Sahu N, Bhan C, Singh J (2020a) Removal of fluoride from an aqueous solution by batch and column process using activated carbon derived from iron infused *Pisum sativum* peel: characterization, isotherm, kinetics study. Environ Eng Res 26(4):1–11. https://doi.org/10.4491/eer.2020.241

Sahu S, Mallik L, Pahi S et al (2020b) Facile synthesis of poly o-toluidine modified lanthanum phosphate nanocomposite as a superior adsorbent for selective fluoride removal: a mechanistic and kinetic study. Chemosphere 252:126551. https://doi.org/10.1016/j.chemosphere.2020.126551

Saikia P, Bharali RK, Baruah HK (2017) Kinetic and thermodynamic studies for fluoride removal using a novel bio-adsorbent from possotia (*Vitex negundo*) leaf. J Anal Sci Technol 8(1):1–9. https://doi.org/10.1186/s40543-017-0132-y

Sengupta P, Saha S, Banerjee S, Dey A, Sarkar P (2020) Removal of fluoride ion from drinking water by a new Fe (OH)$_3$/nano CaO impregnated chitosan composite adsorbent. Polym Plast Technol Mater 59(11):1191–1203. https://doi.org/10.1080/25740881.2020.1725567

Shen T, Gao M (2019) Gemini surfactant modified organo-clays for removal of organic pollutants from water: a review. Chem Eng J 375:121910. https://doi.org/10.1016/j.cej.2019.121910

Singh J, Singh P, Singh A (2016) Fluoride ions vs removal technologies: a study. Arab J Chem 9(6):815–824. https://doi.org/10.1016/j.arabjc.2014.06.005

Solanki YS, Agarwal M, Gupta S, Shukla P, Gupta AB (2019) Fluoride removal performance of a synthesized adsorbent. J Energy Environ Sustain 7:17–20

Uddin MK, Ahmed SS, Naushad M (2019) A mini update on fluoride adsorption from aqueous medium using clay materials. Desalin Water Treat 145:232–248. https://doi.org/10.5004/dwt.2019.23509

Waghmare SS, Arfin T (2015) Fluoride removal from water by various techniques. Int J Innov Sci Eng Technol 2(3):560–571

Wambu EW, Kurui AJ (2018) Fluoride adsorption onto soil adsorbents: the role of pH and other solution parameters. In: Oshunsanya S (ed) Soil pH for nutrient availability and crop performance. IntechOpen, London, pp 31–44. https://doi.org/10.5772/intechopen.74652

Wendimu G, Zewge F, Mulugeta E (2017) Aluminium-iron-amended activated bamboo charcoal (AIAABC) for fluoride removal from aqueous solutions. J Water Process Eng 16:123–131. https://doi.org/10.1016/j.jwpe.2016.12.012

Yadav KK, Kumar S, Pham QB, Gupta N, Rezania S, Kamyab H, Talaiekhozani A (2019) Fluoride contamination, health problems and remediation methods in Asian groundwater: a comprehensive review. Ecotoxicol Environ Saf 182:109362. https://doi.org/10.1016/j.ecoenv.2019.06.045

Yang H, Wang Y, Bender J, Xu S (2019) Removal of arsenate and chromate by lanthanum-modified granular ceramic material: the critical role of coating temperature. Sci Rep 9(1):1–12. https://doi.org/10.1038/s41598-019-44165-8

Zhang S, Lyu Y, Su X, Bian Y, Yu B, Zhang Y (2016) Removal of fluoride ion from groundwater by adsorption on lanthanum and aluminum loaded clay adsorbent. Environ Earth Sci 75(5):401. https://doi.org/10.1007/s12665-015-5205-x

Zhang RL, Xu J, Gao L, Wang Z, Wang B, Qin SY (2020) Performance and mechanism for fluoride removal in groundwater with calcium modified biochar from peanut shell. Sci Adv Mater 12(4):492–501. https://doi.org/10.1166/sam.2020.3620